Molecular recognition and modification of the 30S ribosome by the aminoglycoside-resistance methyltransferase NpmA

Jack A. Dunkle, Kellie Vinal, Pooja M. Desai, Natalia Zelinskaya, Miloje Savic, Dayne M. West, Graeme L. Conn[1], and Christine M. Dunham[1]

Department of Biochemistry, Emory University School of Medicine, Atlanta, GA 30322

Edited by Rachel Green, The Johns Hopkins University, Baltimore, MD, and approved March 19, 2014 (received for review February 13, 2014)

Aminoglycosides are potent, broad spectrum, ribosome-targeting antibacterials whose clinical efficacy is seriously threatened by multiple resistance mechanisms. Here, we report the structural basis for 30S recognition by the novel plasmid-mediated aminoglycoside-resistance rRNA methyltransferase A (NpmA). These studies are supported by biochemical and functional assays that define the molecular features necessary for NpmA to catalyze m^1A1408 modification and confer resistance. The requirement for the mature 30S as a substrate for NpmA is clearly explained by its recognition of four disparate 16S rRNA helices brought into proximity by 30S assembly. Our structure captures a "precatalytic state" in which multiple structural reorganizations orient functionally critical residues to flip A1408 from helix 44 and position it precisely in a remodeled active site for methylation. Our findings provide a new molecular framework for the activity of aminoglycoside-resistance rRNA methyltransferases that may serve as a functional paradigm for other modification enzymes acting late in 30S biogenesis.

antibiotic resistance | base flipping | RNA modification

The ribosome is a complex macromolecular machine responsible for protein synthesis in all cells. The high sequence and structural conservation of key functional centers, such as those for decoding and peptidyl transferase activity, make the ribosome a major target for antibiotics (1, 2). Aminoglycosides predominantly bind the ribosome in the decoding center of the 30S subunit and reduce the fidelity of decoding (3, 4). Chemical probing and structures of the aminoglycoside-bound ribosomal A-site model RNA and 30S subunit localize the binding site within helix 44 (h44) (3, 5–7). Aminoglycoside binding causes two functionally critical rRNA nucleotides, A1492 and A1493, to flip from h44 and adopt positions that typically only arise from cognate tRNA-mRNA pairing (8). This drug-bound state thus allows for selection of incorrect tRNAs by the ribosome and results in aberrant protein production.

Aminoglycosides have historically been powerful tools in the clinic, and although they remain in use today, the breadth of their application has been limited by toxicity and their replacement by alternative antibiotics. However, the emergence of pathogenic bacteria resistant to these alternatives has led to a reevaluation of aminoglycoside use, particularly against Gram-negative pathogens (9, 10). Whereas efforts to circumvent aminoglycoside toxicity issues may broaden their application, any reprieve may be limited by the continued spread of resistance to this class of antibiotics. Currently, the most widely disseminated aminoglycoside resistance determinants are drug modification enzymes, but 16S rRNA methyltransferases that modify the drug-binding site have recently emerged as a significant threat (10, 11). Unlike the drug-modifying enzymes that typically act on a limited number of aminoglycosides, the two nucleobase modifications introduced by 16S rRNA aminoglycoside-resistance methyltransferases confer class-wide resistance to these drugs.

Aminoglycoside-resistance 16S rRNA methyltransferases are divided into two subfamilies that modify either G1405 or A1408 within h44 to produce m^7G1405 or m^1A1408, respectively (12). Although originally identified in Gram-positive aminoglycoside-producing actinomycetes, enzymes catalyzing these modifications have been acquired by human and animal pathogens, where they confer high-level, broad-spectrum resistance to classical and next-generation aminoglycosides (10, 13). Enzymes of producer and pathogen origin have low sequence identity (typically ~25–30%), but recent structural studies have revealed high structural conservation within each subfamily (14–17). G1405 and A1408 modifying enzymes possess a common class I methyltransferase S-adenosyl-L-methionine (SAM)–binding fold containing a seven-stranded, β-sheet core (Fig. S1*A*). However, they differ markedly in their auxiliary domains and/or regions linking the core β-strands. The G1405 methyltransferases have a large N-terminal domain that forms two α-helical subdomains, whereas the A1408 enzymes possess a short β-hairpin at their N terminus and large internal extensions between β-strands β5/β6 and β6/β7. Despite these differences, both the G1405 and A1408 enzymes have an absolute requirement for the mature 30S as their substrate (18, 19). However, the molecular details of recognition and specific target nucleotide modification remain elusive.

Here, we report the 3.8-Å resolution X-ray crystal structure of the *Thermus thermophilus* (*Tth*) 30S ribosome subunit complexed

Significance

Increasing global spread of antibiotic resistance among pathogenic bacteria threatens a postantibiotic era in healthcare. Detailed studies of resistance mechanisms are therefore urgently required. The ribosome is a major antibiotic target, but bacteria can acquire resistance by modification of drug-binding sites. Here, we describe, to our knowledge, the first molecular snapshot of bacterial ribosome recognition by a pathogen-derived, aminoglycoside-resistance rRNA methyltransferase. Our results support a model in which initial rigid docking on a highly conserved ribosome tertiary surface drives conformational changes in the enzyme that capture the target base within a remodeled active site. Extreme conservation of the ribosome-docking surface suggests there is no impediment to the spread of this resistance activity but also presents a target for specific inhibitor development.

Author contributions: G.L.C. and C.M.D. designed research; J.A.D., K.V., P.M.D., N.Z., M.S., and D.M.W. performed research; J.A.D., G.L.C., and C.M.D. analyzed data; and J.A.D., G.L.C., and C.M.D. wrote the paper.

The authors declare no conflict of interest.

This article is a PNAS Direct Submission.

Data deposition: The atomic coordinates and structure factors have been deposited in the Protein Data Bank, www.pdb.org (PDB ID code 4OX9).

[1]To whom correspondence may be addressed. E-mail: gconn@emory.edu or christine.m.dunham@emory.edu.

This article contains supporting information online at www.pnas.org/lookup/suppl/doi:10.1073/pnas.1402789111/-/DCSupplemental.

with the novel plasmid-mediated 16S rRNA methyltransferase A (NpmA), an aminoglycoside-resistance determinant identified in the clinical *Escherichia coli* strain ARS3 (19). Together with complementary biochemical and functional studies, our results provide, to our knowledge, the first molecular framework for recognition and modification by an aminoglycoside-resistance rRNA methyltransferase that may be broadly applicable to other 16S rRNA modification enzymes that act on the 30S subunit.

Results and Discussion

Directed RNA Structure Probing Orients NpmA on h44. To determine the position and orientation of NpmA on the *E. coli* 30S subunit in solution, we performed directed hydroxyl radical probing using NpmA site-specifically derivatized with Fe(II)-1-(p-bromoacetamidobenzyl)–EDTA (Fe-BABE) (*Materials and Methods*). Five single-Cys proteins representing a broad distribution of the probe across the NpmA surface were selected for directed structure probing experiments (Fig. S2). Three Fe(II)-modified NpmA proteins (NpmA-S89C, NpmA-E149C, and NpmA-K151C) produced unique but partially overlapping 16S rRNA strand scission patterns in h44 at nucleotides 1409–1412, 1419–1423, and 1481–1484 (Fig. S2*D*). These results clearly position the NpmA surface containing S89, E149, and K151 adjacent to h44, placing the extended region linking strands β5 and β6 (β5/6 linker) into close proximity with the target site. These results are in extremely good agreement with our *Tth* 30S–NpmA crystal structure (described below), which additionally identifies an extensive interaction surface with regions of 16S more distant from h44 and A1408.

Overview of the 30S–NpmA–Sinefungin Complex. The X-ray crystal structure of the *Tth* 30S subunit complexed with NpmA and the SAM analog sinefungin was determined at a resolution of 3.8 Å (Fig. 1, Fig. S1 *B* and *C*, and Table S1). Remarkably, this structure was obtained by soaking preformed 30S crystals (20) with the 25.2-kDa NpmA complexed with sinefungin. NpmA docks on h44 and the adjacent rRNA structure of a single 30S subunit, distant from any crystal contacts. Before crystallization experiments, we showed that NpmA methylates *Tth* 30S ribosomes as efficiently as those from *E. coli*, confirming that our structure would represent an active state of the enzyme (Fig. S1*D*). These data, together with the corroborating evidence from our directed RNA probing using *E. coli* 30S, clearly demonstrate the veracity of our structure, which captures NpmA in a "pre-catalytic state," poised for methyl transfer to A1408.

NpmA forms an extensive interaction surface (1,557 Å^2) with the 16S rRNA structure formed by the juxtaposition of helices h24, h27, h44, and h45 (Fig. 1 *B* and *C*). These four 16S rRNA helices are far apart in primary sequence but, in the context of the mature 30S subunit fold, form a single complex surface

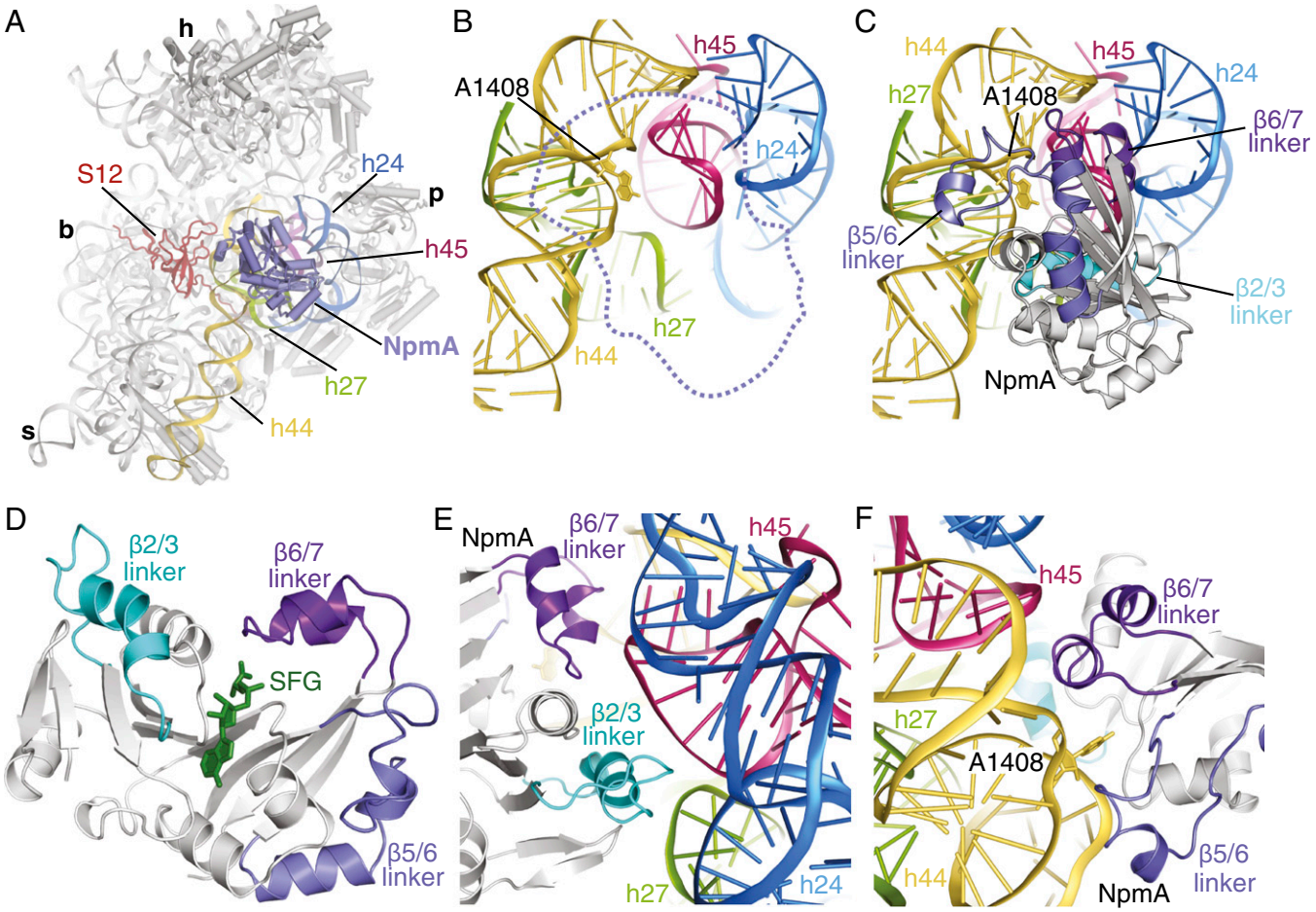

Fig. 1. X-ray crystal structure of the 30S subunit–NpmA complex. (*A*) NpmA (purple) binds at the 30S decoding center and interacts with four 16S rRNA helices: h24 (blue), h27 (green), h44 (yellow), and h45 (magenta). Features of the 30S subunit are labeled as head (h), platform (p), spur (s), and body (b). (*B*) Close-up view of the complex 16S rRNA tertiary structure recognized by NpmA with the interaction surface highlighted (dotted line). A1408 is shown as sticks. The A1408 target nucleotide is shown as sticks. (*C*) Same view of the 16S rRNA surface but with the bound NpmA shown as a cartoon. (*D*) NpmA regions mediating most contacts with 16S rRNA are highlighted: β2/3 linker (cyan), β5/6 linker (slate), and β6/7 linker (purple). Sinefungin (SFG) is shown as sticks (green). (*E* and *F*) The β2/3 linker makes intimate contacts with h24, h27, and h45, whereas the β6/7 linker recognizes the junction of h44 and h45. The β5/6 linker makes an additional contact to h44 below A1408.

recognized by NpmA. This observation provides a clear structural rationale for the requirement of the fully assembled 30S as the substrate for NpmA and other A1408 methyltransferases. Despite the proximity of protein S12 to A1408 in the ribosomal A site (Fig. 1*A*), the 30S–NpmA interaction is mediated exclusively by recognition of the sugar-phosphate backbone of the conserved rRNA surface. In addition to verifying the location and likely role of the NpmA β5/6 linker adjacent to h44 as determined from RNA probing, the structure identifies the NpmA β2/3 and β6/7 linker regions as playing critical roles in 30S docking (Fig. 1 *B*–*F*). NpmA captures A1408 flipped from h44 and precisely positioned in its active site for catalysis. Our structure and comparisons with free NpmA suggest that docking and concerted conformational changes within the two unique extended regions (β5/6 and β6/7 linkers) mediate specific recognition of A1408 and control of catalysis through active site remodeling.

Identification of Residues Critical for NpmA Activity. A limited number of NpmA residues proposed to be critical for SAM binding, recognition of the mature 30S, or catalysis have been investigated previously by mutagenesis and kanamycin minimum inhibitory concentration (MIC) measurements in *E. coli* (17). Mutation of two absolutely conserved Trp residues (W107 and W197) resulted in complete loss of resistance, clearly pointing to their critical role in catalysis or substrate positioning. However, no single point mutations of residues proposed to be involved in rRNA recognition reduced resistance. In contrast, similar studies on KamB, the A1408 methyltransferase from the tobramycin producer *Streptoalloteichus tenebrarius*, identified several functionally important Arg and Lys residues (15). We reasoned that the extensive 30S–methyltransferase interaction surface must, in the case of NpmA, have sufficient redundancy that at least one contact may be lost without an observable effect on the level of kanamycin resistance. Therefore, we adopted two parallel strategies. First, each individual target mutation was made in two contexts, WT enzyme and a functionally compromised mutant (NpmA-E146A; kanamycin MIC of 256–512 μg/mL). Second, two clusters of adjacent target residues, K66/K67 and K70/K71, were mutated at the same time (Table S2).

In the context of the NpmA-E146A mutant, individual mutation of residues distributed across the small N-terminal extension, as well as the β2/3, β5/6, and β6/7 linkers, reduced resistance to kanamycin to 8–16 μg/mL (Table S2). With two notable exceptions discussed below (R153E and R207E), each of these mutations produced no measurable decrease in activity when made in the WT context. These results indicate that each of these residues contributes to the total binding interaction but that loss of any one contact is sufficiently compensated for by the remaining extensive interactions. Notably, three mutations (K8, F92, and Y145) made in the NpmA-E146A background did not reduce the kanamycin MIC further, indicating that second mutations made in the E146A context do not always inactivate the enzyme. These analyses demonstrate the importance of the entire buried NpmA surface for recognition and binding of the 30S.

The NpmA β2/3 linker is rich in Lys residues that, as a group, are well conserved among the A1408 methyltransferases. Although individual mutation of these residues in the WT enzyme had no observable phenotype, kanamycin resistance was modestly reduced by double mutations (K66E/K67E or K70E/K71E) and completely ablated by the quadruple mutant (Table S2). As described below, these residues bridge the four disparate 16S rRNA helices contacted by NpmA and, collectively, appear to play the predominant role in initial docking of NpmA onto the 16S rRNA surface.

Sequence-Independent Tertiary Contacts Distant from the Methylation Site Direct 30S–NpmA Recognition. The regions connecting β-strands 2 and 3 (β2/3 linker) and β-strands 6 and 7 (β6/7 linker) of NpmA are primarily responsible for recognition of the complex rRNA surface of the 30S (Fig. 1 *D*–*F*). The β2/3 linker contains an α-helix (α3) followed by a loop structure that, together, comprise a highly basic extended surface sandwiched between the core of NpmA and the 30S subunit (Fig. 1*E* and Fig. S3*A*). This surface directly contacts all four rRNA helices bound by NpmA (h24, h27, h44, and h45). Helix α3 abuts h44 and forms two electrostatic contacts via K66 and K67 to h27 and h45, respectively, whereas the lysine-rich loop forms interactions via K70, K71, and K74 that measure the juxtaposition of h24 and h45 (Fig. 2 *A* and *B*). Mutation of these residues decreased kanamycin resistance (Table S2), confirming their important role in 30S binding.

The β2/3 linker is conformationally identical in the 30S-bound and free states (Fig. S4), suggesting it is a rigid structural element preformed for recognition of the complex electronegative surface created by h24, h27, and the h44/h45 junction. In contrast, the β6/7 linker, which sits in a deep cleft between h44 and h45, undergoes a substantial local conformational change upon 30S binding (Fig. S4). Electrostatic and van der Waals contacts are made with the apex of the h45 tetraloop, whereas R205 and R207 of NpmA reach into the minor groove of h44 and form electrostatic contacts with the phosphate of A1408 (Fig. 2*C*). The most

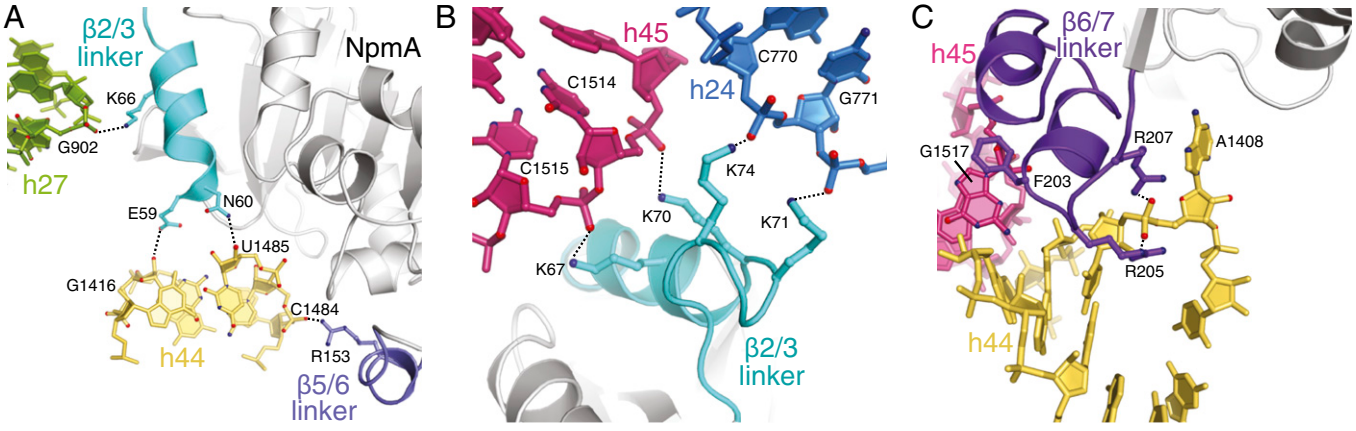

Fig. 2. NpmA makes multiple contacts across the complex 16S rRNA surface formed by h24, h27, h44, and h45. (*A*) NpmA β2/3 linker (cyan) forms an electrostatic contact with h27 (green) and hydrogen-bonding interactions to a ribose group on each strand of h44 (yellow) that measure the minor groove width. An additional electrostatic contact is formed at an adjacent h44 residue by the β5/6 linker (slate). (*B*) Highly basic loop in the NpmA β2/3 linker recognizes the juxtaposition of h45 (magenta) and h24 (blue) through multiple electrostatic interactions with rRNA backbone. (*C*) NpmA β6/7 linker (purple) reaches into a narrow cleft between h44 and h45 of 16S rRNA. F203 stacks with the tetraloop of h45, whereas R205 and R207 reach into the h44 minor groove to make electrostatic interactions with the phosphate group of the target nucleotide A1408, which is flipped out of the h44 base stack.

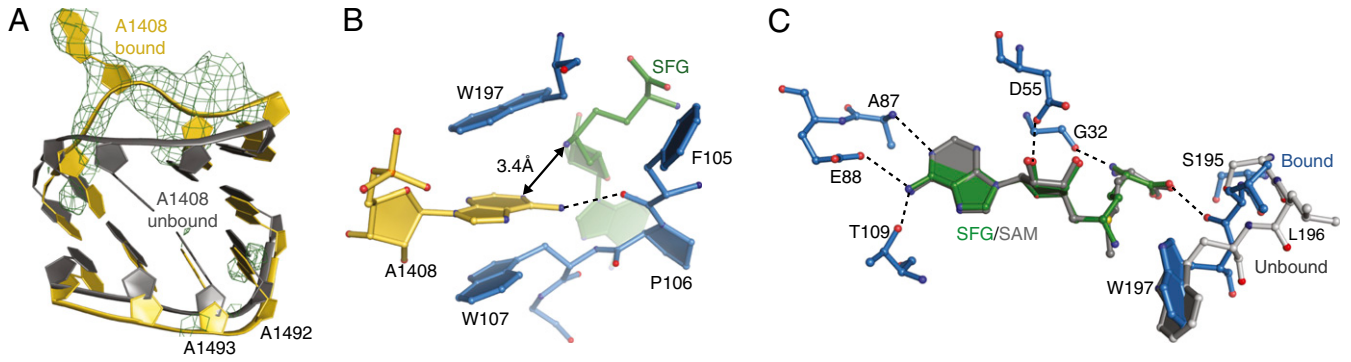

Fig. 3. A1408 is flipped from h44 and sequestered in a remodeled NpmA active site. (*A*) When NpmA is bound (yellow), A1408 is flipped from h44 as shown by the isomorphous difference electron density (green mesh), contoured at 3σ. The structure of the same region of h44 in the absence of NpmA is shown for comparison (PDB ID code 1J5E; gray). (*B*) A1408 is intimately sequestered within the NpmA active site (blue sticks). Residues W107 and W197 form π-stacking interactions with A1408, and the backbone carbonyl of F105 forms a hydrogen bond to the adenine N6. (*C*) Comparison of the cofactor-binding pocket with SFG (green) in the 30S–NpmA–SFG complex structure and SAM (gray) in the free NpmA–SAM complex (PDB ID code 3MTE). The cofactor orientation (rmsd = 0.3 Å) and interactions with amino acids are maintained. One additional hydrogen-bonding interaction between the carbonyl of L196 and the SFG carboxyl group specific to the cofactor mimic in the 30S-bound structure results from the local reorganization of the β6/7 linker.

significant conformational change upon 30S binding occurs in the NpmA β5/6 linker. This change results in an electrostatic contact between R153 of the β5/6 linker and the nonbridging phosphate oxygen of C1484 in h44 (Fig. 2*A*). C1484 is located approximately a half-turn of the helix away from A1408 in the center of a stretch of non-Watson–Crick base pairs that imparts an unusual RNA backbone geometry for recognition by NpmA.

Despite its extensive interactions across four rRNA helices and around the target nucleotide, NpmA makes only a single rRNA sequence-specific interaction. The universally conserved P106 introduces a sharp kink in the NpmA backbone that orients the F105 carbonyl group to hydrogen bond with the N6 amine of A1408 (Fig. 3). This single interaction between A1408 and F105 appears to serve as the only mechanism by which NpmA probes the identity of the target base. Limited need for direct discrimination of the target base may reflect the near-universal conservation of A1408 in bacteria. Consistent with this concept, mutation of P106 has no impact on NpmA activity (17) and F105 is not strictly conserved (Fig. S5). Together, these observations suggest that NpmA is an intrinsically promiscuous enzyme whose specificity is controlled primarily by 30S substrate recognition and subsequent allosteric changes that organize the active site.

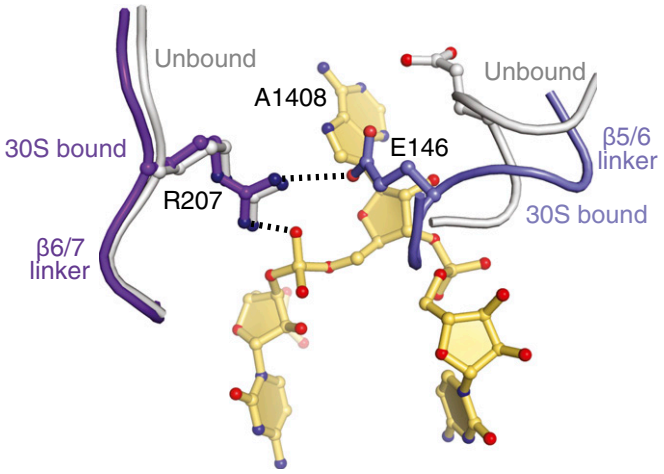

Fig. 4. Conformational change in the β5/6 linker positions E146 to support the role of R207 in A1408 base flipping. Arginine 207 is conformationally static in the 30S-bound (purple) and free (gray) forms (PDB ID code 3MTE) of NpmA but would sterically clash with the phosphate group of A1408 in the absence of base flipping. Rearrangement of the β5/6 linker (slate) brings E146 into position to form a charged hydrogen bond with R207 that acts as a buttress, forcing A1408 to flip to avoid the steric clash.

Precatalytic State Shows A1408 Flipped from h44 and Poised for Methylation. In the presence of the catalytically inert SAM analog sinefungin, the 30S–NpmA complex is trapped in a precatalytic state revealing the molecular mechanism of A1408 positioning in the NpmA active site (Fig. 3 and Fig. S6). Initial unbiased F_O-F_O difference electron density maps clearly show A1408 flipped out of h44 and rotated ~180° around its helical axis (Fig. 3*A*). Two arginine residues within the β6/7 linker, R205 and R207, make electrostatic interactions at the A1408 phosphate that appear to promote or stabilize the necessary RNA backbone structural reorganization (Fig. 2*C*). Our NpmA functional data show that only R207 is critical for activity (Table S2), indicating that it must be the main driver of local conformational changes that flip A1408 from h44. Precise positioning of R207 also appears to be dependent upon a charged hydrogen bond made with E146 (Fig. 4), the mutation of which also substantially reduces NpmA activity (Table S2). Although the position of R207 is similar in the 30S-bound and free NpmA structures [Protein Data Bank (PDB) ID code 3MTE] (15), the major structural rearrangement of the β5/6 linker is required to bring E146 into position to fulfill this role. Therefore, in addition to positioning R153 for recognition of h44, the structural reorganization of the β5/6 linker (Fig. 4 and Fig. S4) directly promotes A1408 base flipping.

Removal of A1408 from the base-stacked environment of h44 is stabilized by π-stacking of the adenine base between two universally conserved and functionally critical tryptophan residues, W107 and W197, in the NpmA active site (Fig. 3*B*). These residues position the adenine N1 directly adjacent to the NpmA-bound SAM analog. Comparison of the free (PDB ID code 3MTE) and 30S-bound NpmA structures indicates that a reorientation of W107 and W197 is required to accommodate the target nucleotide into the NpmA active site (Fig. S6 *A* and *B* and Movie S1). Mutation of either Trp to Ala or Phe completely abolishes NpmA activity (15, 17), confirming their critical role in precise positioning of the target nucleotide.

Our structure of the 30S–NpmA complex reveals an NpmA active site that is poised for catalysis with the A1408 N1 atom positioned 3.4 Å away from the sinefungin amino group that replaces the reactive methyl of the authentic cofactor SAM (Fig. 3*B*). The positioning of substrate and coenzyme is consistent with an S_N2 reaction mechanism with N1 as the nucleophile (Fig. S6 *E* and *F*). Comparison of the positions of sinefungin and SAM in

the 30S–NpmA and free NpmA–SAM complex (PDB ID codes 3P2K and 3MTE) (15, 17) demonstrates that all interactions delineating the cofactor binding pocket are maintained. However, the local structural reorganization of the β6/7 linker causes it to approach the methionyl moiety of the cofactor more closely, and reorientation of L196 positions its backbone carbonyl to make the only additional hydrogen-binding interaction with the cofactor in the 30S-bound form of NpmA (Fig. 3*C* and Fig. S6 *C* and *D*). This 30S-induced interaction with the cofactor may influence NpmA activity by specifically enhancing its affinity for SAM and/or promoting product release, exploiting the >30-fold higher affinity of free NpmA for the reaction byproduct S-adenosylhomocysteine (17).

Mechanisms of Molecular Recognition, Conformational Adaptation, and A1408 Modification. We propose that a sequence of events occurs during the 30S–NpmA molecular recognition process to activate catalysis and ensure target site specificity. Initial docking of NpmA exploits two complementary rigid surfaces, the complex rRNA tertiary structure formed by helices h24, h27, h44, and h45 and the NpmA β2/3 linker. This interaction promotes conformational changes in the NpmA β5/6 and β6/7 linkers, allowing R207 to capture h44 at the A1408 phosphate, promoting flipping of A1408. Finally, A1408 is sequestered in an intimate binding pocket completed by W107 and W197 closure onto the adenosine ring in an induced-fit mechanism that precisely orients it for attack of the ε-methyl of SAM. In support of this model, recent studies of the DNA methyltransferase M.HhaI offer a precedent for base flipping before active site closure (21).

DNA methyltransferases promote base flipping by destabilizing the helix around the target nucleotide and stabilizing the flipped state by replacement of DNA base pairing and stacking with protein–DNA interactions (22). In contrast to the Watson–Crick base-paired target of DNA methyltransferases, A1408 is located in h44 opposite A1492/A1493 but forms only a single hydrogen bond to A1493. Nucleotides A1492/A1493 are essential to the high fidelity of decoding and are themselves conformationally dynamic to allow for inspection of the mRNA-tRNA pair (8). Thus, A1408 may be more readily flipped by virtue of the inherent dynamics in this region of h44 such that the major role of NpmA is to capture and stabilize the flipped conformation by the concerted action of initial docking and the critical molecular interactions mediated by NpmA residues R207, W107, and W197.

Mechanistic Conservation and Variation Among Aminoglycoside-Resistance 16S rRNA Methyltransferases. Because the A1408 aminoglycoside-resistance methyltransferases are highly divergent in sequence, we asked whether the 30S recognition and base-flipping mechanisms revealed by our structure might be conserved among these enzymes. Despite having only ∼30% identity in amino acid sequence, the NpmA and KamB structures are essentially identical, with the only significant conformational differences found in the β5/6 linker (15). Mutagenesis of KamB implicated the β2/3 and β6/7 linkers in a putative 30S-binding surface, and alignment of KamB onto the 30S-bound NpmA structure confirms that these regions are positioned to interact with the same complex rRNA surface formed by h24, h27, h44, and h45 (Figs. S3*B* and S7 and Table S2). The strong functional conservation of residues important for both NpmA and KamB activity indicates that the 30S docking and target nucleotide recognition mechanisms, mediated primarily by the β2/3 and β6/7 linkers, respectively, are common to all A1408 methyltransferases. Absolute conservation of the functionally critical Trp residues (107 and 197 in NpmA) also indicates that A1408 base flipping is a common mechanistic feature.

Although these global recognition features are likely conserved, comparison of the 30S–NpmA structure and 30S–KamB model, taken with functional data on both enzymes, suggests that they differ in the specific molecular details of their action. For example, we identify here a single NpmA residue (R207) that is critical for base flipping via its interaction with the A1408 phosphate group, but mutation of the equivalent residue in KamB (R203) has minimal effect on activity (Table S2). Additionally, there is no obvious equivalent in the KamB β5/6 linker of NpmA residue E146, which supports R207 in its role in A1408 base flipping. Instead, KamB activity is ablated by mutation of R196 or R201 (15), suggesting that in KamB, they act in concert to fulfill the role of NpmA R207. Thus, although these enzymes are functionally equivalent, in that they both methylate N1 of A1408 and exploit the same 30S features for substrate recognition, they differ in the molecular details of their action. Whether the A1408 methyltransferase family adopts further heterogeneous molecular mechanisms built upon a common mode of global recognition will require detailed structural and functional analyses of additional enzymes in this family.

The members of the G1405 subfamily of aminoglycoside-resistance 16S rRNA methyltransferases differ substantially in their structures compared with enzymes targeting A1408. Although these enzymes are built upon the same SAM-binding core fold, they lack equivalents of the NpmA β5/6 and β6/7 extensions that are critical for 30S recognition by A1408 methyltransferases. Additionally, although the α-helix of the β2/3 linker is preserved, it is occluded by the large N-terminal extension in the G1405 enzymes that appears to direct 30S interactions (14, 16). Nonetheless, given the proximity of G1405 and A1408 and their common requirement for the intact 30S as a substrate, the G1405 enzymes must presumably exploit similar features of the conserved 16S rRNA tertiary surface.

Modification Enzymes May Target Nucleotides in the Decoding Center by a Common Mechanism. Modification of 16S rRNA confers antibiotic resistance but also serves to regulate ribosome biogenesis and to fine-tune protein synthesis (23). Modifications of 16S rRNA include 10 mono- or dimethylated nucleotides and a single pseudouridine that form two distinct clusters within the 30S subunit (24, 25): lining the mRNA tunnel and the decoding center, adjacent to the aminoglycoside-resistance modifications (Fig. S8). There is an apparent dichotomy in substrate requirement between the enzymes responsible for these two modification clusters. Enzymes acting around the mRNA tunnel typically methylate naked 16S RNA or some form of pre-30S subunit. In contrast, like the aminoglycoside-resistance methyltransferases, the six enzymes responsible for the cluster of methylations within the decoding center require a fully assembled 30S subunit. We predict that each of these enzymes will exploit features of the h24, h27, and h44/h45 tertiary surface to achieve their target recognition and specificity. Our results thus provide, to our knowledge, the first molecular basis for what may be a common mechanism of 30S particle recognition in a sequence-independent but tertiary structure-dependent manner.

The cryo-EM structure of one of these intrinsic 16S rRNA methyltransferases, RsmA (formerly KsgA), bound to the 30S was determined recently (26). RsmA acts late in 30S biogenesis, dimethylating A1518 and A1519 in h45 in a step that has been proposed to signal the end of subunit assembly (27). The cryo-EM structure of the 30S-RsmA complex offered initial insights suggesting that specificity may be governed by the juxtapositioning of multiple rRNA helices. However, based on this low-resolution analysis, it was not possible to judge whether sequence-dependent contacts are made in addition to the recognition of RNA tertiary structure. In RsmA, the core SAM-binding fold is embellished with a large C-terminal domain that is positioned to interact with h24 and h27 of 16S rRNA and may direct specificity by orienting the enzyme active site over the target nucleotides. Our structure of the 30S–NpmA complex provides a precedent for specific recognition in the absence of any sequence specific contacts and reliance solely on interactions with the sugar-phosphate backbone of the juxtaposed rRNA helices that form in the mature particle. Steric accessibility of the target site may explain why NpmA and RsmA rely on recognition of tertiary features, whereas other modification enzymes that act early in ribosome biogenesis recognize sequence. Further

structures will need to be determined to verify whether this theme, linking recognition with the stage of ribosome maturity, generally holds true.

Feasibility of Horizontal Gene Transfer to Other Pathogens. Extensive evidence indicates that antibiotic resistance genes are ancient and exist within microbial communities in pristine environments (28–30). Acquired resistance genes in pathogens are presumed to originate from these sources, with their prevalence enriched by exposure to antibiotic (mis)use in agriculture and medicine. An important question is therefore, how easily might other pathogenic microbes acquire and exploit resistance determinants like NpmA?

The strong conservation of the complex tertiary surface exploited by NpmA suggests it is very likely to be active in all bacterial species without significant adaptation. Indeed A1408 and G1405 enzymes have been found to be fully active in all heterologous systems tested to date (31–33). Together, these data and our mechanistic insights into NpmA action suggest that there exists no major impediment to the rapid spread of A1408 aminoglycoside-resistance activity among pathogenic bacterial populations. However, the highly conserved nature of the A1408 methyltransferase docking site also presents a novel target for development of specific inhibitors of these resistance determinants.

Materials and Methods

Fe-BABE–Directed 16S rRNA Structure Probing. Directed hydroxyl radical probing of 16S rRNA using single cysteine NpmA mutants derived with Fe-BABE was performed essentially as previously described (27, 34). Further details can be found in *SI Materials and Methods*.

NpmA Mutagenesis and Kanamycin MIC Assays. The ability of NpmA mutants to support bacterial growth in the presence of kanamycin (0–1,024 μg/mL) was measured in liquid culture. The MIC was determined as the lowest kanamycin concentration that fully inhibited growth. Further details can be found in *SI Materials and Methods*.

Structural Determination of the 30S–NpmA–Sinefungin Complex. The *Tth* 30S subunits were purified, crystallized, and cryoprotected, and *E. coli* NpmA protein was purified as previously described (20, 35). The NpmA–sinefungin complex was incubated with preformed 30S crystals and flash-frozen in liquid nitrogen. X-ray diffraction data were collected from two well-diffracting crystals at the Northeastern Collaborative Access Team (NE-CAT) beamline 24-ID-C of the Advanced Photon Source (Table S1). Data reduction and merging were completed with X-ray Detector Software (XDS) (36). Crystallographic refinement was performed in PHENIX (37), followed by iterative rounds of manual rebuilding in Coot (38). Figure preparation was performed with PyMOL (39).

ACKNOWLEDGMENTS. We thank J. Marquez for technical assistance and D. Reines and X. Cheng for discussion and comments. This work was funded by National Institutes of Health (NIH)-National Institute of Allergy and Infectious Diseases Grant R01-AI088025 (to G.L.C.) and, in part, by NIH-National Institute of General Medical Sciences Grant R01-GM093279 (to C.M.D.). C.M.D. is a Pew Scholar in the Biomedical Sciences. This work is based on research conducted at the Advanced Photon Source on the Northeastern Collaborative Access Team (NE-CAT) beamlines, which is supported by NIH-National Center for Research Resources Award RR-15301, and at the Southeastern Regional Collaborative Access Team beamline. Use of the Advanced Photon Source, an Office of Science User Facility operated for the US Department of Energy (DOE) Office of Science by Argonne National Laboratory, was supported by the US DOE under Contract DE-AC02-06CH11357.

1. Wilson DN (2014) Ribosome-targeting antibiotics and mechanisms of bacterial resistance. *Nat Rev Microbiol* 12(1):35–48.
2. Franceschi F (2007) Back to the future: The ribosome as an antibiotic target. *Future Microbiol* 2(6):571–574.
3. Moazed D, Noller HF (1987) Interaction of antibiotics with functional sites in 16S ribosomal RNA. *Nature* 327(6121):389–394.
4. Davies J, Gorini L, Davis BD (1965) Misreading of RNA codewords induced by aminoglycoside antibiotics. *Mol Pharmacol* 1(1):93–106.
5. Fourmy D, Recht MI, Blanchard SC, Puglisi JD (1996) Structure of the A site of Escherichia coli 16S ribosomal RNA complexed with an aminoglycoside antibiotic. *Science* 274(5291):1367–1371.
6. Carter AP, et al. (2000) Functional insights from the structure of the 30S ribosomal subunit and its interactions with antibiotics. *Nature* 407(6802):340–348.
7. Vicens Q, Westhof E (2002) Crystal structure of a complex between the aminoglycoside tobramycin and an oligonucleotide containing the ribosomal decoding a site. *Chem Biol* 9(6):747–755.
8. Ogle JM, et al. (2001) Recognition of cognate transfer RNA by the 30S ribosomal subunit. *Science* 292(5518):897–902.
9. Falagas ME, Grammatikos AP, Michalopoulos A (2008) Potential of old-generation antibiotics to address current need for new antibiotics. *Expert Rev Anti Infect Ther* 6(5):593–600.
10. Jackson J, Chen C, Buising K (2013) Aminoglycosides: How should we use them in the 21st century? *Curr Opin Infect Dis* 26(6):516–525.
11. Ramirez MS, Tolmasky ME (2010) Aminoglycoside modifying enzymes. *Drug Resist Updat* 13(6):151–171.
12. Conn GL, Savic M, Macmaster R (2009) Resistance to antibiotics in bacteria through modification of nucleosides in 16S ribosomal RNA. *DNA and RNA Modification Enzymes: Comparative Structure, Mechanism, Functions, Cellular Interactions and Evolution*, ed Grosjean H (Landes Bioscience, Austin, TX).
13. Wachino J, Arakawa Y (2012) Exogenously acquired 16S rRNA methyltransferases found in aminoglycoside-resistant pathogenic Gram-negative bacteria: An update. *Drug Resist Updat* 15(3):133–148.
14. Schmitt E, Galimand M, Panvert M, Courvalin P, Mechulam Y (2009) Structural bases for 16 S rRNA methylation catalyzed by ArmA and RmtB methyltransferases. *J Mol Biol* 388(3):570–582.
15. Macmaster R, Zelinskaya N, Savic M, Rankin CR, Conn GL (2010) Structural insights into the function of aminoglycoside-resistance A1408 16S rRNA methyltransferases from antibiotic-producing and human pathogenic bacteria. *Nucleic Acids Res* 38(21):7791–7799.
16. Husain N, et al. (2010) Structural basis for the methylation of G1405 in 16S rRNA by aminoglycoside resistance methyltransferase Sgm from an antibiotic producer: A diversity of active sites in m7G methyltransferases. *Nucleic Acids Res* 38(12):4120–4132.
17. Husain N, et al. (2011) Structural basis for the methylation of A1408 in 16S rRNA by a panaminoglycoside resistance methyltransferase NpmA from a clinical isolate and analysis of the NpmA interactions with the 30S ribosomal subunit. *Nucleic Acids Res* 39(5):1903–1918.
18. Zarubica T, Baker MR, Wright HT, Rife JP (2011) The aminoglycoside resistance methyltransferases from the ArmA/Rmt family operate late in the 30S ribosomal biogenesis pathway. *RNA* 17(2):346–355.
19. Wachino J, et al. (2007) Novel plasmid-mediated 16S rRNA m1A1408 methyltransferase, NpmA, found in a clinically isolated Escherichia coli strain resistant to structurally diverse aminoglycosides. *Antimicrob Agents Chemother* 51(12):4401–4409.
20. Clemons WM, Jr., et al. (2001) Crystal structure of the 30 S ribosomal subunit from Thermus thermophilus: Purification, crystallization and structure determination. *J Mol Biol* 310(4):827–843.
21. Matje DM, Krivacic CT, Dahlquist FW, Reich NO (2013) Distal structural elements coordinate a conserved base flipping network. *Biochemistry* 52(10):1669–1676.
22. Huang N, Banavali NK, MacKerell AD, Jr. (2003) Protein-facilitated base flipping in DNA by cytosine-5-methyltransferase. *Proc Natl Acad Sci USA* 100(1):68–73.
23. Decatur WA, Fournier MJ (2002) rRNA modifications and ribosome function. *Trends Biochem Sci* 27(7):344–351.
24. Dunin-Horkawicz S, et al. (2006) MODOMICS: A database of RNA modification pathways. *Nucleic Acids Res* 34(Database issue):D145–D149.
25. Machnicka MA, et al. (2013) MODOMICS: A database of RNA modification pathways—2013 update. *Nucleic Acids Res* 41(Database issue):D262–D267.
26. Boehringer D, O'Farrell HC, Rife JP, Ban N (2012) Structural insights into methyltransferase KsgA function in 30S ribosomal subunit biogenesis. *J Biol Chem* 287(13):10453–10459.
27. Xu Z, O'Farrell HC, Rife JP, Culver GM (2008) A conserved rRNA methyltransferase regulates ribosome biogenesis. *Nat Struct Mol Biol* 15(5):534–536.
28. Allen HK, et al. (2010) Call of the wild: Antibiotic resistance genes in natural environments. *Nat Rev Microbiol* 8(4):251–259.
29. D'Costa VM, et al. (2011) Antibiotic resistance is ancient. *Nature* 477(7365):457–461.
30. Pruden A, Arabi M, Storteboom HN (2012) Correlation between upstream human activities and riverine antibiotic resistance genes. *Environ Sci Technol* 46(21):11541–11549.
31. Holmes DJ, Drocourt D, Tiraby G, Cundliffe E (1991) Cloning of an aminoglycoside-resistance-encoding gene, kamC, from Saccharopolyspora hirsuta: Comparison with kamB from Streptomyces tenebrarius. *Gene* 102(1):19–26.
32. Galimand M, Sabtcheva S, Courvalin P, Lambert T (2005) Worldwide disseminated armA aminoglycoside resistance methylase gene is borne by composite transposon Tn1548. *Antimicrob Agents Chemother* 49(7):2949–2953.
33. Savic M, Lovric J, Tomic TI, Vasiljevic B, Conn GL (2009) Determination of the target nucleosides for members of two families of 16S rRNA methyltransferases that confer resistance to partially overlapping groups of aminoglycoside antibiotics. *Nucleic Acids Res* 37(16):5420–5431.
34. Culver GM, Noller HF (2000) Directed hydroxyl radical probing of RNA from iron(II) tethered to proteins in ribonucleoprotein complexes. *Methods Enzymol* 318:461–475.
35. Zelinskaya N, Rankin CR, Macmaster R, Savic M, Conn GL (2011) Expression, purification and crystallization of adenosine 1408 aminoglycoside-resistance rRNA methyltransferases for structural studies. *Protein Expr Purif* 75(1):89–94.
36. Kabsch W (2010) Integration, scaling, space-group assignment and post-refinement. *Acta Crystallogr D Biol Crystallogr* 66(Pt 2):133–144.
37. Echols N, et al. (2012) Graphical tools for macromolecular crystallography in PHENIX. *J Appl Cryst* 45(Pt 3):581–586.
38. Emsley P, Lohkamp B, Scott WG, Cowtan K (2010) Features and development of Coot. *Acta Crystallogr D Biol Crystallogr* 66(Pt 4):486–501.
39. Schrodinger LLC (2010) The PyMOL Molecular Graphics System, Version 1.3r1.